ETH zürich

ETH Library

Granular Biomaterials as Bioactive Sponges for the Sequestration and Release of Signaling Molecules

Journal Article

Author(s):
Emiroglu, Dilara Börte; Singh, Apoorv; Marco-Dufort, Bruno; Speck, Noël; Rivano, Pier Giuseppe; Oakey, John; Nakatsuka, Nako; de Mello, Andrew J.; Labouesse, Celine; Tibbitt, Mark W.

Publication date:
2024-10-07

Permanent link:
https://doi.org/10.3929/ethz-b-000678438

Rights / license:
Creative Commons Attribution-NonCommercial 4.0 International

Originally published in:
Advanced Healthcare Materials 13(25), https://doi.org/10.1002/adhm.202400800

This page was generated automatically upon download from the ETH Zurich Research Collection.
For more information, please consult the Terms of use.

Check for updates

ADVANCED HEALTHCARE MATERIALS
www.advhealthmat.de

Granular Biomaterials as Bioactive Sponges for the Sequestration and Release of Signaling Molecules

*Dilara Börte Emiroglu, Apoorv Singh, Bruno Marco-Dufort, Noël Speck, Pier Giuseppe Rivano, John S. Oakey, Nako Nakatsuka, Andrew J. deMello, Céline Labouesse, and Mark W. Tibbitt**

A major challenge for the regeneration of chronic wounds is an underlying dysregulation of signaling molecules, including inflammatory cytokines and growth factors. To address this, it is proposed to use granular biomaterials composed of jammed microgels, to enable the rapid uptake and delivery of biomolecules, and provide a strategy to locally sequester and release biomolecules. Sequestration assays on model biomolecules of different sizes demonstrate that granular hydrogels exhibit faster transport than comparable bulk hydrogels due to enhanced surface area and decreased diffusion lengths. To demonstrate the potential of modular granular hydrogels to modulate local biomolecule concentrations, microgel scaffolds are engineered that can simultaneously sequester excess pro-inflammatory factors and release pro-healing factors. To target specific biomolecules, microgels are functionalized with affinity ligands that bind either to interleukin 6 (IL-6) or to vascular endothelial growth factor A (VEGF-A). Finally, disparate microgels are combined into a single granular biomaterial for simultaneous sequestration of IL-6 and release of VEGF-A. Overall, the potential of modular granular hydrogels is demonstrated to locally tailor the relative concentrations of pro- and anti-inflammatory factors.

1. Introduction

Wound healing processes are tightly regulated by the activity of a wide array of pro- and anti-inflammatory factors.[1] While wounds that originate from acute injuries normally heal in a timely and organized manner, chronic wounds are characterized by impaired repair mechanisms.[2] This often involves dysregulation of the immune system combined with defective migration and/or proliferation of resident cells (such as keratinocytes), preventing the restoration of the original tissue structure and homeostasis.[3] Cytokines are instructional immunomodulatory components of the wound microenvironment, mediating the initial pro-inflammatory phase of the healing process. However, dysregulation of several cytokines, such as interleukin 6 (IL-6), IL-1β, and tumor necrosis factor (TNF)-α, are associated with prolonged inflammation and delayed wound healing.[4] Accordingly, addressing the dysregulation of these crucial signaling molecules is an attractive approach to accelerate the healing of chronic wounds.

Several approaches have been developed to improve wound healing therapies including skin substitutes, cell delivery, and biomaterial-based strategies.[5–7] Long-term survival of allograft skin substitutes and the risk of rejection due to the immune response by the host tissue represent a challenge for their clinical translation.[8,9] While these approaches offer some potential for the treatment of chronic wounds, they highlight the need for targeted and personalized treatments. Biomaterials-based

D. B. Emiroglu, A. Singh, B. Marco-Dufort, N. Speck, P. G. Rivano, C. Labouesse, M. W. Tibbitt
Macromolecular Engineering Laboratory
Department of Mechanical and Process Engineering
ETH Zurich
Sonneggstrasse 3, Zurich 8092, Switzerland
E-mail: mtibbitt@ethz.ch

D. B. Emiroglu, A. J. deMello
deMello Laboratory
Department of Chemical and Bioengineering
ETH Zurich
Vladimir-Prelog-Weg, 1–5/10, Zurich 8093, Switzerland

J. S. Oakey
Department of Chemical & Biological Engineering
University of Wyoming
1000 E. University Ave, Laramie, WY 82071, USA

N. Nakatsuka
Laboratory of Biosensors and Bioelectronics
Institute for Biomedical Engineering
ETH Zurich
Gloriastrasse 37/39, Zurich 8092, Switzerland

The ORCID identification number(s) for the author(s) of this article can be found under https://doi.org/10.1002/adhm.202400800

© 2024 The Author(s). Advanced Healthcare Materials published by Wiley-VCH GmbH. This is an open access article under the terms of the Creative Commons Attribution-NonCommercial License, which permits use, distribution and reproduction in any medium, provided the original work is properly cited and is not used for commercial purposes.

DOI: 10.1002/adhm.202400800

approaches are promising in this respect as they form 3D microenvironments that mimic critical features of natural extracellular matrix (ECM) and can promote tissue repair.[10–12] While tunable design features of synthetic hydrogels make them attractive candidates as wound healing scaffolds, their nanoscale porosity restricts their exchange with the tissue environment, limiting mass transfer between the biomaterial and surrounding fluids as well as cell migration. As an alternative approach, monolithic (bulk) hydrogel networks have been replaced with micrometer-scale hydrogel particles (microgels) that can be jammed to form a porous scaffold, which can promote cell infiltration and facilitate biomolecule diffusion.[13–16] Such granular hydrogels have been shown to outperform bulk hydrogels by improving wound closure in healthy skin and alleviating the immunogenic reaction associated with traditional bulk hydrogels.[17,18] Granular hydrogels have further been used for the controlled delivery of IL-10 to promote macrophage activation and heterogenous growth factor organization using heparin microgel islands.[19,20] There is a growing interest in leveraging the modular nature of granular hydrogels for tissue regeneration; however, few of these methods enable immune modulation via regulation of multiple cytokines. In particular, the possibility to sequester counterproductive factors and release productive factors simultaneously has not been demonstrated. We propose that the modular design of granular biomaterials can enable this, offering local control over biomolecule concentrations.

The ECM contains molecules that can regulate the activity of growth factors and cytokines. Notably, synthetic matrices can be engineered with immune activating cues, such as glycosaminoglycan (GAG) and heparin domains, that promote regeneration.[21–23] These sites confer an overall negative charge to the matrices and can electrostatically bind certain biomolecules, controlling their local concentration and bioactivity.[24,25] For example, poly(ethylene glycol) (PEG)-based hydrogels have been synthesized with heparin derivatives to trap cytokines within tissues, neutralizing the chemoattractant function of monocyte chemoattractant protein-1 (MCP-1) and IL-8 when applied onto excisional wounds.[26] While this sequestration effect has been shown to reduce the influx of immune cells into the wound, TNF-α, IL-1β, and IL-6 showed negligible binding to the hydrogels due to their reduced affinity to heparin.[26] For these specific cytokines, another approach is to tether antibodies to PEG microgels. PEG microgels functionalized with antibodies against IL-6 were used to detect IL-6 secretion in a diagnostic assay.[27] In another study, microgels were functionalized with antibodies against TNF-α, and were ultimately able to reduce TNF-α toxicity in colorectal adenocarcinoma cells.[28] These approaches show the potential of engineering ECM inspired biomaterials for the capture of cell-secreted cytokines and the control of resident cell behavior, retarding the diffusion of cytokines in the environment and preventing engagement with receptors.

To combine the benefits of granular hydrogels and cytokine sequestration, we engineered granular hydrogels that have sufficient interface and mass transfer with the surrounding environment to act as a bioactive sponge to neutralize unfavorable signaling molecules that may persist in the inflammatory healing environment and deliver favorable signaling molecules (**Figure 1**). Specifically, we designed a versatile and modular platform to be used as an injectable and porous scaffold for potential wound healing applications. Owing to the interconnected, macroporous nature of granular hydrogels, these biomaterials provided more rapid diffusion of model biomolecules of varying sizes than standard hydrogel biomaterials. The incorporation of selective ligands in the form of DNA aptamers with high affinity to IL-6 allowed cytokine capture from the soluble matrix environment. In addition, we combined the sequestration capability of the granular hydrogels with the release of pro-angiogenic factors through the modular combination of distinct microgels in a single granular biomaterial. We show that cell activity scales with the concentration of sequestered IL-6 and released VEGF-A from the microgels. Our results highlight the potential of modular granular hydrogels as immunomodulatory biomaterials that could be used for improved healing of acute and chronic wounds.

2. Results

To design an immunomodulatory granular biomaterial, we first synthesized a versatile and injectable granular hydrogel platform that could serve as an ECM mimic. The granular hydrogels consisted of microgels composed of 8-arm poly(ethylene glycol) (PEG) macromers ($M_n \approx 10\,000$ g mol^{-1}) end-functionalized with norbornene (NB) and a di-thiol linker (DTT). Microgels were formed using microfluidic emulsification of the gel precursor solution, PEGNB, DTT, and the photoinitiator lithium-phenyl-2,4,6-trimethylbenzoylphosphinate (LAP), and thiol–ene photopolymerization upon exposure to ultraviolet light ($\lambda = 365$ nm, $I = 10$ mW cm^{-2}, $t = 60$ s). This fabrication method resulted in spherical microgels of uniform size, ≈75 µm diameter.[14] The microgels had a final shear storage modulus in the range of $G' \approx 6$–40 kPa (5–10 wt% PEG) (Figure S1, Supporting Information). After washing and jamming the particles, macroporous granular hydrogels formed with interconnected porosity. As the constituent microgel building blocks were jammed via transient physical contacts, the macroscopic material was able to flow under shear deformation, rendering the hydrogels moldable and self-healing.[14]

2.1. Diffusion of Model Molecules into Granular Hydrogels

To investigate the potential of granular hydrogels to sequester biomolecules, we characterized the diffusion of model molecules of varying sizes in both bulk and granular hydrogels prepared using the same polymer precursor solution (8-arm PEG-NB/DTT, 5–10 wt%; 45 µL). The gels were then incubated with model biomolecules to model diffusion of diverse nutrients, proteins, and signaling molecules into the hydrogels. The model molecules were rhodamine B (Rh-B; a small molecule with molecular weight (MW) = 480 g mol^{-1}; 1 mg mL^{-1}), lysozyme (a model bioactive enzyme; MW = 14 000 g mol^{-1}; 2 mg mL^{-1}), and fluorescein isothiocyanate conjugated bovine serum albumin (FITC-BSA; a serum protein; MW = 66 000 g mol^{-1}; 1 mg mL^{-1}). We used absorbance-based assays to measure the concentration of molecules over time and infer their diffusion properties. Sequestration assays on granular hydrogels revealed substantial differences in the mass transport (diffusion) of the model biomolecules. In all cases, the supernatant concentration was initially at its maximum and decreased over time as the molecules

© 2024 The Author(s). Advanced Healthcare Materials published by Wiley-VCH GmbH

21922659, 2024, 25, Downloaded from https://onlinelibrary.wiley.com/doi/10.1002/adhm.202400800 by Eth Zurich, Wiley Online Library on [15/10/2024]. See the Terms and Conditions (https://onlinelibrary.wiley.com/terms-and-conditions) on Wiley Online Library for rules of use; OA articles are governed by the applicable Creative Commons License

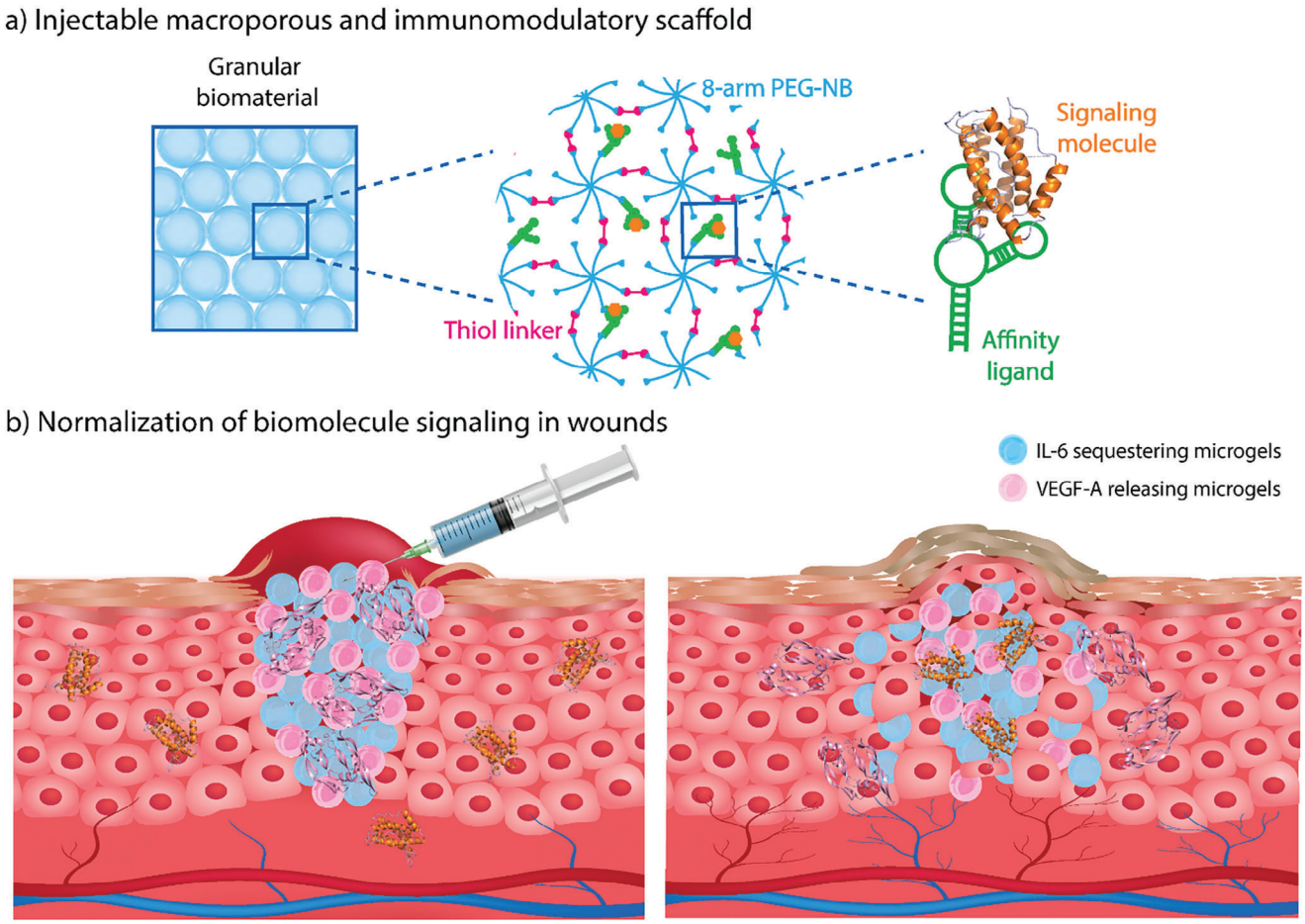

Figure 1. Immunomodulatory granular hydrogels for the healing of chronic wounds. A) Granular hydrogels consist of microgel building blocks that are jammed into a macroscopic scaffold. Microgels can be functionalized with ligands with specific affinity to targeted signaling molecules, allowing their capture or release to modulate their bioactivity. B) Injectable granular hydrogels can be applied to a wound as a dressing, where diffusion and capture of inflammatory cytokines combined with the release of pro-angiogenic factors could improve wound healing outcomes. The granular hydrogel can be a combination of different microgel populations, each functionalized with affinity ligands that target different biomolecules. In this study, we combined IL-6 sequestering microgels (blue) and VEGF-A releasing microgels (pink).

diffused into the hydrogels (**Figure** 2a–c). The diffusion rate for the small molecule (Rh-B) was comparable for both bulk and granular hydrogels and independent of the network cross-linking density, reaching a plateau during the first 8 h. This behavior was expected, since Rh-B is a small molecule that migrates freely and rapidly through the polymer network in both bulk and granular hydrogels. The hydrogel mesh size is known to affect diffusivity of molecules, as physical interactions between the polymer network and biomolecule govern the migration through the material.[29] When the hydrogel mesh size is larger than the molecule (r_{mesh} / $r_{molecule} > 1$), diffusivity can be approximated by the Stokes–Einstein equation $D = k_b T/6\pi\eta r_{molecule}$ where k_b is the Boltzmann constant, T is the temperature, and η is the dynamic viscosity of the solution.[30]

In contrast to Rh-B, the diffusion rate as well as the total amount of molecule in the supernatant at the end of the sequestration assays differed for both lysozyme and FITC-BSA between bulk and granular hydrogels, approaching a plateau at 100 h for lysozyme (Figure 2b). The diffusion coefficient scales with biomolecule size, which partially explains the slower diffusion and long equilibration times, but the diffusive behavior cannot be explained solely by the Stokes–Einstein equation. Granular hydrogels exhibited faster uptake rates compared with bulk networks, suggesting that the biomolecule transport profiles differed because of variations in hydrogel topology. Here, both the increase in biomolecule size and changes in hydrogel topology originating from the inherent macroporosity altered the mass transfer rates. Indeed, the inclusion of macropores in a polymer network can dramatically influence the transport properties, enabling convection.[29] The mesh size of the polymer network also influenced the transport, indicating that biomolecule transport happened within the void space and polymer network simultaneously. Only for the high molecular weight biomolecule did hindrance effects seem to occur due to the smaller mesh size of the polymer network (Figure 2c). These results suggest that granular hydrogels can increase the rate of macromolecular uptake, and their interconnected porosity can be harnessed to sequester biologically relevant large biomolecules (MW > 14 000 g mol^{-1}) while allowing free diffusion of small nutrients.

© 2024 The Author(s). Advanced Healthcare Materials published by Wiley-VCH GmbH

21922659, 2024, 25, Downloaded from https://onlinelibrary.wiley.com/doi/10.1002/adhm.202400800 by Eth Zurich, Wiley Online Library on [15/10/2024]. See the Terms and Conditions (https://onlinelibrary.wiley.com/terms-and-conditions) on Wiley Online Library for rules of use; OA articles are governed by the applicable Creative Commons License

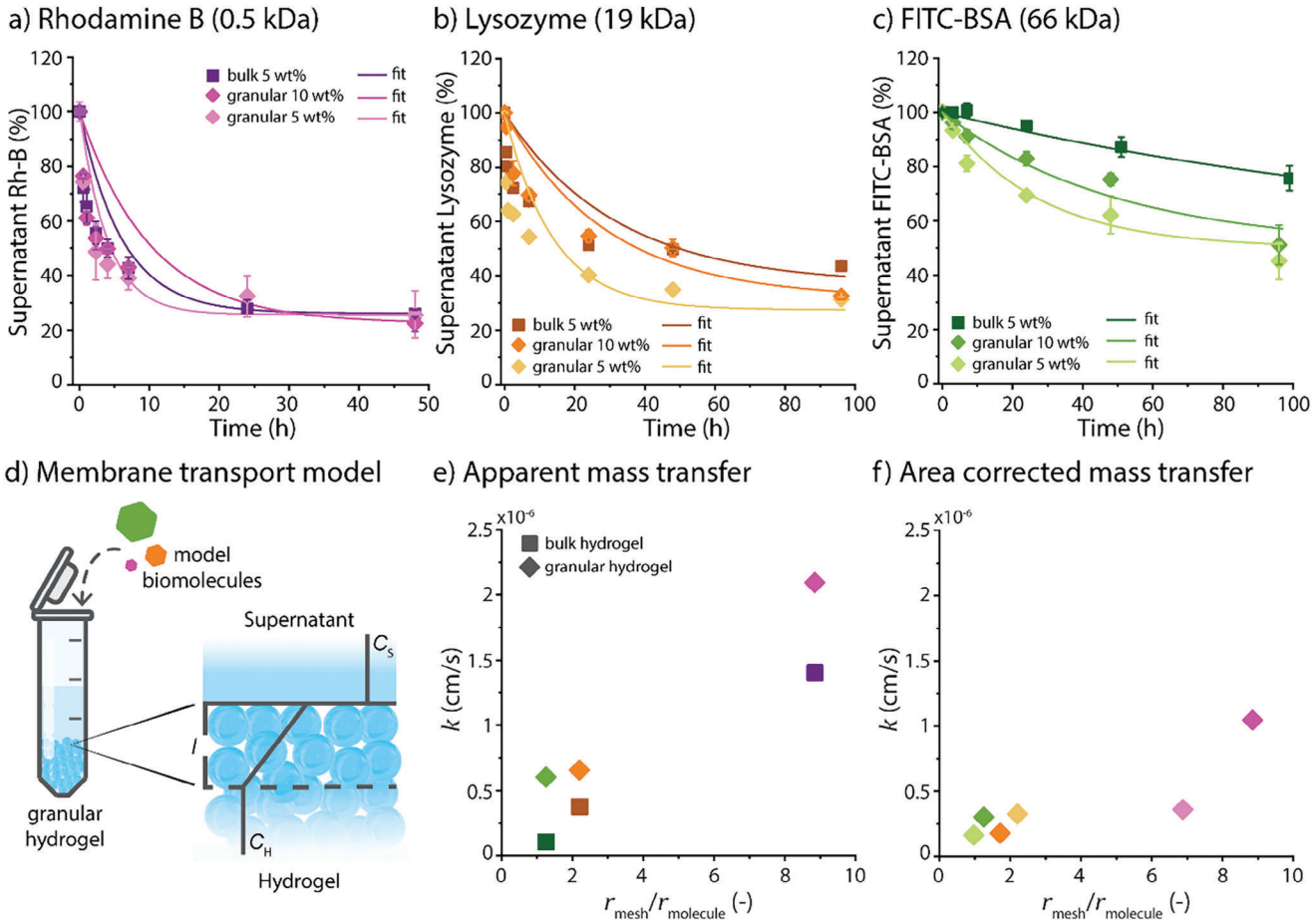

Figure 2. Biomolecule diffusion in granular hydrogels. Transport of model biomolecules into bulk and granular hydrogels (8-arm PEG-NB/DTT, 5–10 wt%; pH 7.4, 25 °C; 45 µL) is facilitated by the presence of interconnected porosity. Diffusion assays for a) Rhodamine B (Rh-B; 1 mg mL^{-1}; 45 µL). b) Lysozyme (2 mg mL^{-1}; 45 µL), and c) Fluorescein isothiocyanate-labeled bovine serum albumin (FITC-BSA; 1 mg mL^{-1}; 45 µL) were performed to study the transport profile of model biomolecules. Supernatant concentrations were assessed via absorbance measurements. A transport model was developed to provide a theoretical framework that explains transport of model biomolecules into hydrogels. d) Schematic representation of the concentration profiles of supernatant, C_S, and hydrogel, C_H across an interface, separated by a hypothetical film of thickness, l. Mass transport coefficients, k, were extracted using the derived analytical model by fitting experimental diffusion curves for each biomolecule. According to our hypothesis, by accounting for the increased surface area available for diffusion, we can appropriately represent the diffusion in granular hydrogels. e) Apparent k for bulk and granular hydrogels with the same composition (8-arm PEG-NB/DTT, 5–10 wt%; pH 7.4, 25 °C). f) Area corrected k for granular hydrogels (8-arm PEG-NB/DTT, 5–10 wt%; pH 7.4, 25 °C. The results are consistent with standard diffusion theories, which state that the transport rate is proportional to network mesh size and inversely proportional to biomolecule size. Data are represented as mean +/− std., $n = 3$.

2.2. Modeling the Enhanced Biomolecule Transport in Granular Hydrogels

Our transport assays demonstrated that the macroporous nature of granular hydrogels enabled more rapid transport of biomolecules into the biomaterial scaffolds. Starting from a framework of mass transfer relations, we applied a simple model to describe the transport behavior exhibited by biomolecules in hydrogels (Section 2.1). We note that in the above assays, the driving force for mass transport is a concentration gradient, where transport across the hydrogel–supernatant interface leads to a variation in concentration of biomolecules in both phases as a function of time. By defining a virtual thin film of thickness l, through which transport occurs across the hydrogel–supernatant interface, we derived an analytical formula that approximates the variation of concentration of biomolecules in the supernatant, C_S, over time (Figure 2d and Section 2.1). Via Equation S11 (Supporting Information), we described C_S as a function of the mass transfer coefficient, k, a single parameter that encompasses the mass transfer properties of the model biomolecules in the considered system. The analytical model qualitatively described the biomolecule uptake in both bulk and granular hydrogels (Figure 2a–c).

The mass transfer coefficient is often defined as a system property of a molecule moving through a hydrogel. However, granular hydrogels comprise jammed microgel building blocks where the packed structure contains void spaces through which free diffusion and convective transport can occur. We assumed that the increased transport rates were predominantly governed by the increased surface area available for transport in granular hydrogels. This is to be expected, as the polymer network that comprises both bulk and microgel scaffolds are equivalent at a

© 2024 The Author(s). Advanced Healthcare Materials published by Wiley-VCH GmbH

21922659, 2024, 25, Downloaded from https://onlinelibrary.wiley.com/doi/10.1002/adhm.202400800 by Eth Zurich, Wiley Online Library on [15/10/2024]. See the Terms and Conditions (https://onlinelibrary.wiley.com/terms-and-conditions) on Wiley Online Library for rules of use; OA articles are governed by the applicable Creative Commons License

fixed polymer density. We estimated the interfacial area, A, of the exposed microgel surfaces at the interface to be approximately twice that of bulk hydrogels. We noted that the extracted k values without this area correction led to an overestimation of mass transfer properties within granular hydrogels (Figure 2e). Area corrected k values for granular hydrogels, plotted against r_{mesh} / $r_{molecule}$, were in agreement with the Stokes–Einstein relationship, i.e., the biomolecule mass transfer coefficient (or equivalently the diffusion rate) was inversely proportional to $r_{molecule}$ (Figure 2f). Moreover, the mass transfer coefficient decreased with polymer network density, indicating slower diffusion and decreased mass transfer in hydrogels with smaller mesh sizes. This schematization of biomolecule transport allowed us to compare the uptake profiles of biomolecules for hydrogels with different topologies (granular and bulk) and cross-linking density and highlighted the potential to design materials that sequester biomolecules based on simple considerations of the underlying transport phenomena.

2.3. Biofunctionalized Granular Sponges Facilitate Sequestration of Inflammatory Cytokines

The use of granular hydrogels presents unique opportunities for immunomodulatory therapies since size, topology, packing density, and biofunctionality can be tailored to control biomolecule diffusion. These properties can be specifically designed to induce anti-inflammatory effects, opening a wide range of strategies for various biomedical applications. In the above sections, we demonstrated that an increased surface area and decreased path length can be effective in controlling the uptake of model biomolecules. Encouraged by these results, we hypothesized that granular hydrogels, when injected into a wound or injury site could modulate the inflammatory response by neutralizing pro-inflammatory signaling factors and/or providing pro-regenerative factors. Studying the uptake, sequestration, and release of inflammatory factors in vitro could therefore provide insights into the potential of granular hydrogels to promote regeneration in vivo. In this context, we first considered the pro-inflammatory cytokine interleukin 6 (IL-6, MW = 21 kDa) due to its well-known role as a mediator of early inflammation in chronic wounds, such as diabetic foot ulcers.[31]

In principle, many relevant biomolecules can be taken up by granular hydrogels through improved transport. By ensuring specific sequestration (and inactivation) of excess pro-inflammatory molecules, the balance between pro- and anti-inflammatory signals could be shifted to promote regeneration. For this purpose, a selective capture mechanism was introduced to increase the residence time within hydrogels. Specifically, we incorporated high affinity ligands (K_d in the nM range) into the polymer backbone in the form of single stranded DNA aptamers that target IL-6 (**Figure 3a**). Aptamers are single-stranded oligonucleotides that can non-covalently bind target molecules with high affinity and specificity.[32] The capture of cytokines via aptamer sequences relies heavily on the proper folding and molecular recognition of the target molecule.[33] To confirm the binding of the aptamer to IL-6 in situ, we employed quartz crystal microbalance with dissipation monitoring (QCM-D, Figure S3a, Supporting Information). A decrease of ≈75 Hz in the resonance frequency of the quartz crystal was observed upon aptamer injection, indicating successful assembly of the thiolated aptamers on the gold surface (Figure S3b, Supporting Information). Rinsing with the buffer did not alter the measured frequency, indicating a covalently modified aptamer layer. Following sequential injections of IL-6 (1 μM), the resonance frequency decreased repeatedly until stability was achieved at 125 Hz, indicating IL-6 binding to the aptamer layer (Figure S3c, Supporting Information). This IL-6 aptamer–target binding was reversible upon multiple injections of the buffer.

Upon validating IL-6 binding, the thiolated aptamer sequences were conjugated to the polymer network (postproduction of the microgels) using thiol–ene chemistry. Microgels were fabricated via the rotisserie emulsification method to increase throughput (Figure S2, Supporting Information). The microgels were prepared by leaving excess thiol reactive NB groups in the cross-linked network, which could then undergo a reaction with the thiol end of the aptamer sequences in the presence of LAP (λ = 365 nm, I = 15 mW cm^{-2}). Aptamer-functionalized gels consisted of 8-arm PEG-NB/DTT networks (5 wt%) with 2.5 μM IL-6-binding aptamer. To verify the integration of aptamers inside the microgels, we used SYBR-gold, a fluorescent dye that intercalates into single-stranded DNA, resulting in a >1000-fold fluorescence enhancement.[34] Images of aptamer-functionalized microgels stained with SYBR-gold showed distinct fluorescence signal confirming the incorporation of the aptamers (Figure 3a). To further demonstrate specific binding of IL-6 to aptamer-functionalized microgels, we performed isothermal titration calorimetry (ITC) measurements (Figure 3b,c; and Figure S4, Supporting Information). The injection curves showed gradual saturation upon IL-6 additions as evidenced by the decreasing heat (associated with binding) measured upon each injection. We then set out to show that the incorporation of these aptamers can serve as affinity agents to modulate the selective capture and retention of cytokines in the hydrogel networks, by measuring the sequestration of IL-6 over time in aptamer-functionalized and non-functionalized granular hydrogels (Figure 3d). In non-functionalized gels, the sequestration rate was close to the transport rate of lysozyme (Figure 2b), which was expected, since both proteins have similar molecular weights. Critically, we observed that the sequestration rate depended on the presence of aptamer sequences, as granular hydrogels with incorporated aptamers exhibited a rapid decrease in IL-6 concentration during the first 6 h and an increased total capture amount as compared with non-functionalized granular hydrogels (Figure 3e).

We next confirmed that the granular hydrogels can also sequester cell-secreted IL-6. For this, we used human keratinocyte cells (HaCaT) in a monolayer. HaCaT cells were treated with 10 ng mL^{-1} TNF-α. TNF-α treatment induced upregulation of inflammatory signals IL-6 and IL-8 at the gene level and IL-6 at protein level (Figure S6, Supporting Information), supporting the establishment of a hyperinflammatory environment. We then used a Transwell assay to simulate the granular hydrogel–tissue interface (Figure S7, Supporting Information). Protein measurements showed that over 48 h, the granular hydrogels sequestered IL-6 (Figure S7, Supporting Information). Uptake was also confirmed by later releasing the sequestered IL-6 from the granular hydrogels (Figure S7, Supporting Information). These results

© 2024 The Author(s). Advanced Healthcare Materials published by Wiley-VCH GmbH

21922659, 2024, 25, Downloaded from https://onlinelibrary.wiley.com/doi/10.1002/adhm.202400800 by Eth Zurich, Wiley Online Library on [15/10/2024]. See the Terms and Conditions (https://onlinelibrary.wiley.com/terms-and-conditions) on Wiley Online Library for rules of use; OA articles are governed by the applicable Creative Commons License

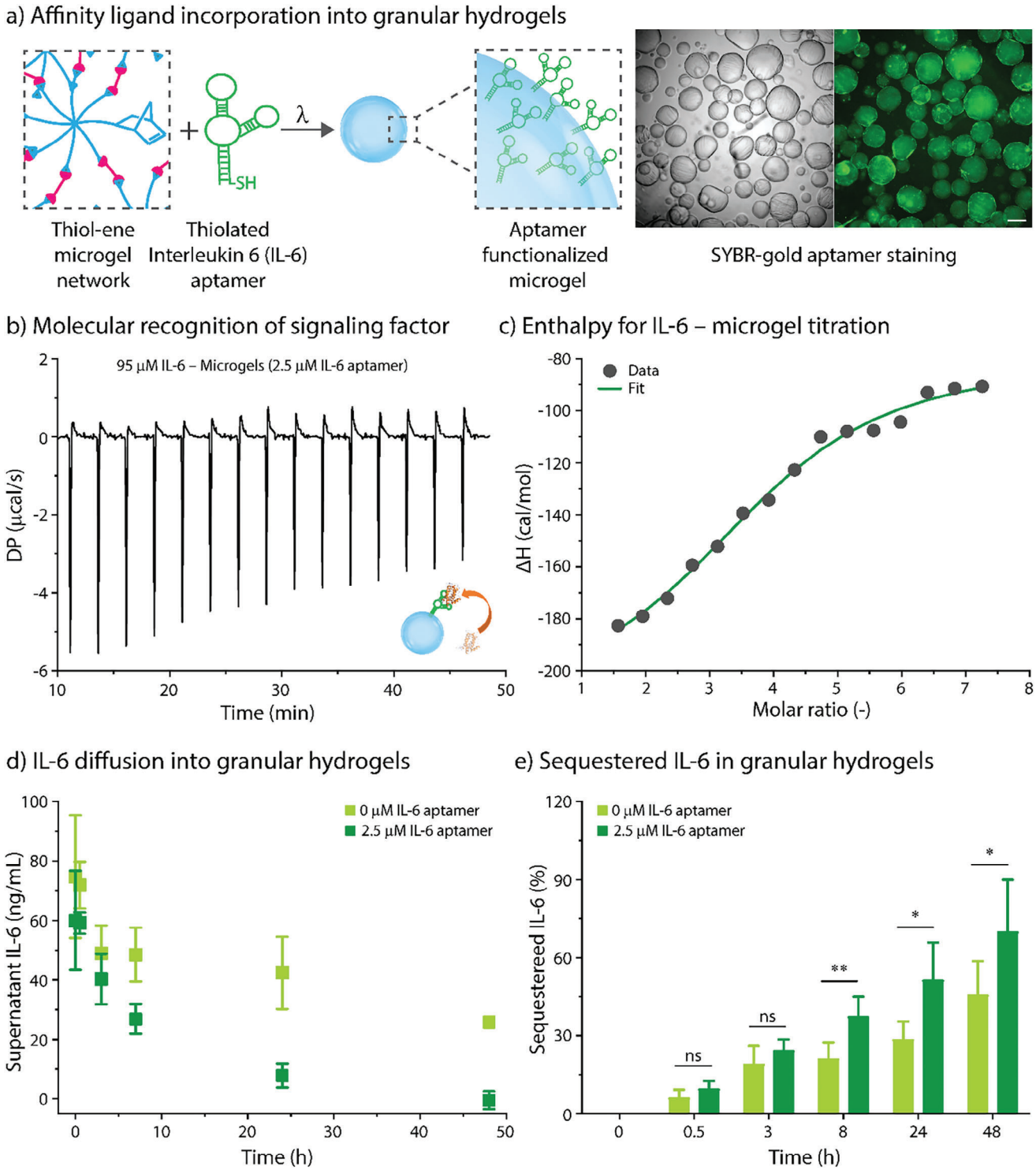

Figure 3. Cytokine sequestration using granular hydrogels. a) Microgels (8-arm PEG-NB/DTT, 5 wt%; pH 7.4) were functionalized with IL-6 aptamer (2.5 µM) sequences through thiol–ene cross-linking. SYBR-gold staining of the aptamer-functionalized microgels (left image: brightfield, right image: fluorescent) showed visibly higher fluorescence intensities. Scale bar, 200 µm. b) Specific binding of IL-6 in microgels was confirmed via isothermal titration calorimetry (ITC), where 95 µM IL-6 was injected to a suspension of microgels (8-arm PEG-NB/DTT, 5 wt%; pH 7.4, 2.5 µM IL-6 aptamer). Binding isotherm from the integrated thermogram fit using the one-site model from MicroCal (Levenberg–Marquardt iterations). c) Enthalpy of IL-6-microgel binding over the sequence of injections of IL-6. d) IL-6 sequestration assays on control nonfunctionalized and aptamer-functionalized granular hydrogels were performed using the same protocol as for model biomolecules with a starting concentration of IL-6 of 200 ng mL^{-1}. Results were analyzed by ELISA. e) Relative amount of IL-6 sequestered by the granular hydrogels over time, averaged over 4 independent experiments. Data are represented as mean +/− std., $n = 3$–4. Statistical analysis was performed using one-tailed paired *t*-test. $*p < 0.05$, $**p < 0.01$, ns not significant.

 © 2024 The Author(s). Advanced Healthcare Materials published by Wiley-VCH GmbH

21922659, 2024, 25, Downloaded from https://onlinelibrary.wiley.com/doi/10.1002/adhm.202400800 by Eth Zurich, Wiley Online Library on [15/10/2024]. See the Terms and Conditions (https://onlinelibrary.wiley.com/terms-and-conditions) on Wiley Online Library for rules of use; OA articles are governed by the applicable Creative Commons License

confirmed the potential of granular hydrogels to act as a cytokine sponge in a biological context.

2.4. Simultaneous Sequestration and Release of Distinct Signaling Molecules

One of the advantages of using granular hydrogels is the possibility to combine populations of microgels with different features into a single modular biomaterial, for example capturing aberrant signaling factors or delivering therapeutic molecules. In the context of chronic wounds, simultaneous capture of inflammatory cytokines and release of pro-regenerative factors is a potential strategy to normalize the signaling environment. To demonstrate this principle, we combined IL-6 sequestering granular hydrogels with vascular endothelial growth factor (VEGF-A)-releasing granular hydrogels. VEGF-A (MW = 19 kDa) is important to promote angiogenesis, an essential step in wound healing. We used a PEG-dithiol linker instead of DTT to increase the mesh size of the polymer networks, thereby facilitating the release of VEGF-A (Figures S2 and S8, Supporting Information). To ensure loading of VEGF-A into the microgels, we incorporated thiolated heparin in the backbone of the hydrogels network (Figure S8a, Supporting Information). Heparin is known to have high affinity to VEGF-A.[35] In addition, by combining IL-6 sequestering microgels and VEGF-A-loaded microgels into a single granular biomaterial, we could modulate the local presentation of IL-6 and VEGF-A (**Figure** 4a). The concentration of IL-6 in the supernatant decreased significantly with aptamer-functionalized microgels (100:0 A:H) as compared with non-aptamer-functionalized microgels (0:100 A:H; Figure 4c). In addition, the concentration of VEGF-A increased with increasing content of VEGF-A-loaded microgels (Figure 4d). These results show that the modular nature of granular hydrogels could allow for tailored modulation of the inflammatory signals in the local microenvironment.

To verify that changes in concentrations of IL-6 and VEGF-A led to changes in local cell signaling, we applied the supernatant onto cells and measured their response (Figure 4b). Human embryonic kidney (HEK) IL-6 reporter cells were used to measure the level of IL-6 signaling by activation of signal transducer and activator of transcription 3 (STAT3) and the subsequent secretion of the embryonic alkaline phosphatase reporter gene (measured by absorbance at 630 nm; Figure S9, Supporting Information). HEK IL-6 signaling decreased with increasing fractions of aptamer-functionalized gels (Figure 4e), confirming that the sequestration of IL-6 lowered the pro-inflammatory signaling activity. The same scaling of IL-6 signaling activity with the amount of aptamer-functionalized microgels was observed for two different initial IL-6 concentrations. Furthermore, human umbilical vascular endothelial cells (HUVECs) expressing GFP (GFP-HUVECs) in the cytoplasm were used to assess, if the released VEGF-A remained bioactive (Figure 4f). HUVECs are dependent on VEGF-A for survival when plated on 2D substrates in the absence of any supporting matrix or supporting stromal cells. The number of surviving HUVECs scaled with the fraction of VEGF-A loaded microgels added, and with the concentration of VEGF-A in the supernatant, up to a plateau (Figure 4f). In contrast, VEGF-A had no effect on IL-6 signaling activity (Figure S11, Supporting Information). These results confirmed that the simultaneous sequestration of IL-6 and release of bioactive VEGF-A can modulate cell signaling.

3. Discussion

To date, the main focus on engineering granular biomaterials for tissue repair has been to take advantage of their porosity to enable cell infiltration and tissue deposition. Our granular biomaterials benefit from these developments while further demonstrating the utility that the engineered porosity and modularity of granular biomaterials provides the ability to selectively sequester and release biomolecules that may be dysregulated in injury or disease. In this study, we engineered a granular biomaterial to specifically impart immunomodulatory effects. We proposed that granular hydrogels would lead to improved diffusion for larger biomolecules owing to the increased interfacial surface area. A recent study investigated the diffusion of biomolecules within nonporous and porous hydrogels using fluorescence recovery after photobleaching and calculated diffusivities by exploiting Fick's Law.[36] Using the same physical framework and calculation of diffusion coefficients for biomolecules, others showed that transport took place more rapidly in microporous annealed particle scaffolds comprising larger microgels compared with smaller microgels.[37] In line with these studies, we observed faster biomolecule uptake in granular biomaterials than in bulk hydrogels. Accounting for enhanced interfacial area available for transport, we qualitatively described how the transport depends on the granular hydrogel topology and inversely scales with biomolecule size. We anticipate that minor changes in size distribution, shape, radial distribution, and packing fraction would have a modest impact on the general area term and not dramatically influence the conclusions of the simple transport model.

We then further demonstrated the dual action capability of our hydrogels to simultaneously capture and release biomolecules, which could be used to normalize inflammatory signaling environments. In wounds, the local concentration of cytokines, such as IL-6 must be tightly controlled. IL-6 is required for keratinocyte proliferation; however, an excess of either of IL-6 is associated with impaired healing.[38,39] Accordingly, the inhibition of excess pro-inflammatory cytokines, such as IL-6, may be an effective approach for the treatment of chronic wounds. We showed that incorporating high affinity aptamer ligands increased the uptake and residence time of IL-6 in the gels. The affinity ligands themselves are not expected to modify the mesh size, due to their low concentration and their inability to participate in cross-linking, but they modify the overall transport behavior of biomolecules via the inclusion of reversible binding sites. IL-6 sequestration using aptamer-functionalized microgels reduced its signaling activity. The attenuated IL-6 signaling observed in HEK sensor cells could translate similarly to epithelial cells in a wound setting and the capture of such pro-inflammatory cytokines may transiently prevent their signaling activity within the wound environment (as the binding is reversible). Furthermore, the same principle could be used to lower the signaling of other cytokines and pro-inflammatory factors.

Previous studies have shown that granular hydrogels can be used to locally release active pro-regenerative factors.[40] To leverage this possibility, we demonstrated here the release over 5 days

© 2024 The Author(s). Advanced Healthcare Materials published by Wiley-VCH GmbH

21922659, 2024, 25, Downloaded from https://onlinelibrary.wiley.com/doi/10.1002/adhm.202400800 by Eth Zurich, Wiley Online Library on [15/10/2024]. See the Terms and Conditions (https://onlinelibrary.wiley.com/terms-and-conditions) on Wiley Online Library for rules of use; OA articles are governed by the applicable Creative Commons License

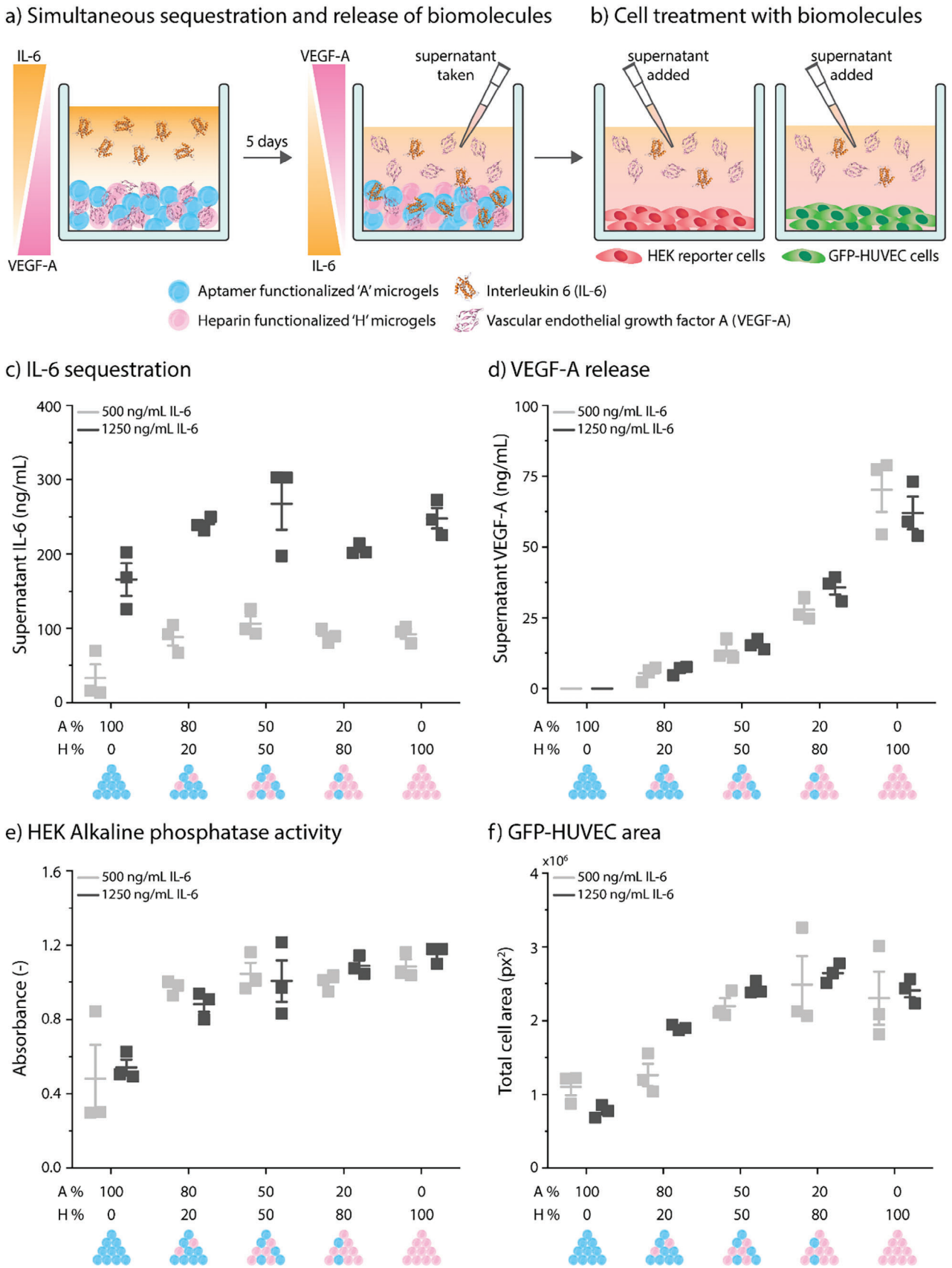

© 2024 The Author(s). Advanced Healthcare Materials published by Wiley-VCH GmbH

21922659, 2024, 25, Downloaded from https://onlinelibrary.wiley.com/doi/10.1002/adhm.202400800 by Eth Zurich, Wiley Online Library on [15/10/2024]. See the Terms and Conditions (https://onlinelibrary.wiley.com/terms-and-conditions) on Wiley Online Library for rules of use; OA articles are governed by the applicable Creative Commons License

of VEGF-A from granular hydrogels functionalized with heparin. The significant advantage of the granular sponge format is that microgels with distinct affinity ligands can be combined into a single biomaterial to simultaneously capture and release factors into the local environment. We demonstrated this concept by sequestering IL-6 while releasing VEGF-A from a single granular biomaterial. To broaden the scope of this approach, the dose effect of varying fractions of differently functionalized microgels and the overall extent of sequestration or release should be further refined. Toward this end, microgels can be tailored to sequester or release multiple signaling molecules, where the relative degree of sequestration and release for each could be modulated by the structure of each microgel, the affinity of the ligands used, and varying the ratio of distinct populations of microgels. Microgels can be functionalized with aptamers (as shown here), antibodies (as shown in previous studies),[41] as well as peptides, GAGs, or other biomolecules that affect the sequestration or release of various relevant biomolecules. As disparate microgels can be jammed together into a coherent, granular biomaterial, mix-and-match granular hydrogels can be engineered for different healing contexts. Of note, the promiscuous binding of GAGs to multiple cytokines and growth factors may reduce the degrees of freedom in controlling signaling activity of individual biomolecules.[26] Nonetheless, this overall constitutes a broadly applicable design strategy for the capture and release of signaling factors using granular hydrogels.

We believe that this approach could prove clinically relevant in the treatment of chronic wounds, due to their immunomodulatory potential and the modularity of this system. Importantly, they would have a local effect only, avoiding the need for systemic delivery of anti-inflammatory drugs or sequestering antibodies. Moreover, they can be easily modified to contain adhesive motifs, providing cues for cell adhesion and cell migration.[42] In addition, their injectability and space-filling properties make them compatible with any wound size and shape. We envision that this innovative approach could be further used to control cytokine activity in time and space for a diverse range of biomedical applications where a combination of immunomodulation and cell–material interactions are needed.

4. Conclusion

In summary, we developed a granular hydrogel sponge that can serve as an immunomodulatory biomaterial. By establishing robust biomolecule diffusion assay and a transport model, we provided insights into the enhanced diffusion characteristics in granular hydrogels. We showed that these granular hydrogels allow for increased diffusion of biomolecules. We further showed that the constituent microgels can be functionalized with affinity ligands, allowing for capture and release of signaling factors, and ultimately a modulation of pro-inflammatory and pro-angiogenic activity. Applying these microgels in a wound or injury site could help to locally normalize the inflammatory signaling. As such, granular hydrogels are promising biomaterials that could be translated into therapeutic applications.

5. Experimental Section

Materials: 8-Arm PEG-NH_2HCl ($M_n \approx 10\,000$ g mol^{-1}) was purchased from JenKem Technology USA. Regenerated cellulose dialysis tubing (1 kDa MWCO) was purchased from Spectrum Labs. Hydrochloric acid (HCl), sodium hydroxide (NaOH), magnesium chloride ($MgCl_2$), sodium dihydrogen phosphate (monobasic; NaH_2PO_4), sodium hydrogen phosphate (dibasic; Na_2HPO_4), 2,2-dihydroxyindane-1,3-dione (ninhydrin), 1-methoxy-2-propyl acetate, polysorbate 20 (Tween 20), bovine serum albumin (BSA), 3,3′,5,5′-tetramethylbenzidine (TMB), 30 wt% hydrogen peroxide solution in H_2O (H_2O_2), sulfuric acid (H_2SO_4), Rhodamine B, Lysozyme, albumin-fluorescein isothiocyanate conjugate (FITC-BSA) were purchased from Sigma-Aldrich. Phosphate-buffered saline (PBS), and tris-buffered saline (TBS) were purchased from ThermoFisher Scientific. Droplet generation oil for probes (Hexane, 3-ethoxy-1,1,1,2,3,4,4,5,5,6,6,6-dodecafluoro-2-(trifluoromethyl)) was purchased from BioRad. IL-6 aptamer sequences, resuspension buffer and folding buffer were bought from Cambio UK (Basepair) and Microsynth AG. Human recombinant Interleukin 6 (IL-6, 10395-HNAE), Human IL-6 Matched ELISA Antibody Pair Set (SEKB10395), human recombinant tumor necrosis factor (TNF-α, 10602-HNAE), human recombinant vascular endothelial growth factor (VEGF165, 11066-HNAH), human VEGF165 matched ELISA Antibody Pair Set (SEK11066), and human FGF-2 (10014-HNAE) were purchased from Sinobiological. Heparin Thiol (MW = 27 kDa) was purchased from Creative PEGworks (HP-211). SYBR-Gold was purchased from Thermofisher (S11494). Transwell inserts were obtained from VWR (6.5 mm; transparent PET membrane; 0.4 µm; cat. no.: 76313-906).

Methods—NMR: ^{1}H 1D NMR spectra were acquired on a Bruker Avance III 400 (Bruker BioSpin GmbH).

Plate Reader: Absorbance measurements were acquired with a Hidex Sense Microplate Reader (Hidex; Turku, Finland) using clear 96-well tissue culture plates (flat bottom; TPP).

Nanodrop One: Absorbance measurements were acquired with a Nanodrop One Microvolume Spectrophotometer (ThermoFisher, Switzerland) at A280 nm wavelength with 5 nm width.

Quartz Crystal Microbalance with Dissipation Monitoring (QCM-D): Measurements were performed using the Q-Sense E4 (Biolin Scientific). The experimental procedure involved the measurement of both the resonance frequency and energy dissipation of the quartz crystal. These

Figure 4. Modular assembly of microgels for dual sequestration and release of signaling factors. The ability for simultaneous sequestration and release of granular biomaterials was demonstrated by preparing a mixture of distinct microgels containing either IL-6 aptamer (A) or heparin (H) binding ligands at varying ratios (100:0, 80:20, 50:50, 20:80, 0:100). a) Microgels were functionalized either with IL-6 aptamer (2.5 µM) or heparin (2.5 µM). For VEGF-A release, heparin-functionalized microgels were loaded with 500 ng mL^{-1} VEGF-A solution overnight. Release solutions for VEGF-A consisting of 500 ng mL^{-1} IL-6 or 1250 ng mL^{-1} IL-6 were added on granular hydrogels and kept for 5 days at 37 °C with mechanical agitation. After 5 days, the supernatant was collected and applied to cells. b) The supernatant was applied to HEK cells (after dilution) and to GFP-HUVECs. c) IL-6 concentration in the supernatant after 5 days for different combinations of aptamer (A) and heparin (H) functionalized microgels ($p < 0.01$ for 500 ng mL^{-1} IL-6, $p < 0.05$ for 1250 ng mL^{-1} IL-6). d) VEGF-A concentration in the supernatant after 5 days for different combinations of aptamer (A) and heparin (H) functionalized microgels ($p < 0.0001$ for 500 ng mL^{-1} IL-6, $p < 0.0001$ for 1250 ng mL^{-1} IL-6). e) Secreted embryonic alkaline phosphatase activity measured by absorbance ($\lambda = 630$ nm) as a readout of IL-6 signaling activity in transformed HEK IL-6 reporter cells ($p < 0.01$ for 500 ng mL^{-1} IL-6, $p < 0.001$ for 1250 ng mL^{-1} IL-6). The HEK cells were incubated with the supernatant of the sequestration/release experiment for 24 h. f) Total cell area of GFP-HUVECs following incubation with the supernatant from the sequestration/release experiment for 48 h ($p < 0.01$ for 500 ng mL^{-1} IL-6, $p < 0.0001$ for 1250 ng mL^{-1} IL-6). Data are represented as mean +/− s.e.m., $n = 3$. Statistical analysis was performed using one-way ANOVA with Tukey's test for post-hoc analysis (see the Supporting Information Tables for detailed p values).

© 2024 The Author(s). Advanced Healthcare Materials published by Wiley-VCH GmbH

21922659, 2024, 25, Downloaded from https://onlinelibrary.wiley.com/doi/10.1002/adhm.202400800 by Eth Zurich, Wiley Online Library on [15/10/2024]. See the Terms and Conditions (https://onlinelibrary.wiley.com/terms-and-conditions) on Wiley Online Library for rules of use; OA articles are governed by the applicable Creative Commons License

measurements were conducted across a range of harmonics, including the fundamental resonance frequency at 5 MHz, as well as the third, fifth, seventh, and ninth overtones. IL-6 aptamer assembly and IL-6 binding experiments were conducted at a concentration of 5 µM in PBS, under a continuous flow of 50 µL min^{-1} via a flow pump (Cole-Parmer GmbH). The QCM-D platform was maintained at a constant temperature of 25 °C, and buffers were degassed prior to injection to avoid bubble formation. The QCM-D sensors with gold (Au) metallization and silicon dioxide (SiO_2) coating (5 MHz, 14 mm diameter) were purchased from MicroVacuum Ltd. (Budapest, Hungary). Prior to use, the chips underwent ultraviolet (UV) ozone treatment for 10 min, followed by sequential sonication for 3 min in acetone, isopropanol, and deionized water (dH_2O), in that order. Chips were then mounted in the QCM-D flow chamber and exposed to aptamer solution (5 µM in PBS) that was pretreated (disulfide reduction and aptamer folding) to ensure free single-stranded thiolated sequences. For functionalization, aptamers were treated for 1 h with 50-fold excess tris(2-carboxyethyl)phosphine (TCEP) relative to the DNA concentration to reduce the disulfide bonds. Then, aptamers were purified using Zeba spin desalting columns (7K MWCO, 0.5 mL, Thermo Fisher Scientific AG). Finally, to ensure unhybridized DNA for assembly, the aptamer solution was heated at 95 °C for 5 min and subsequently cooled to room temperature prior to assembly. The aptamer solution was incubated in the QCM-D until a stable signal was reached with subsequent rinsing steps removing any nonspecific surface adsorption and verifying covalent modification. Upon confirmation of the aptamer assembly on the surface of the quartz crystal, the analyte (1 µM IL-6 in PBS) was exposed to the surface. After maximal binding was reached, the flow chamber was flushed with the buffer to assess reversibility.

Isothermal Titration Calorimetry (ITC): All ITC measurements were performed via a MicroCal PEAQ-ITC (Malvern Panalytical). Before conducting an experiment, the sample cell and injection syringe were rinsed using dH_2O, and the sample cell was dried using methanol. A Hamilton syringe was used to manually load the reference cell with 280 µL of PBS. The sample cell was then similarly loaded with 280 µL of macromolecule. The injection syringe was filled with 40 µL of ligand solution (IL-6 at 95 µM). The injection syringe was then placed into the sample cell. The parameters for the ITC measurement were set in the provided MicroCal software. The injection syringe contained IL-6 solution at 95 µM, and the sample cell contained IL-6 aptamer at 0.25 µM, or IL-6 aptamer loaded microgels at 2.5 µM macromolecule concentration. The reference power was set to 10 µcal s^{-1}, feedback mode was set to high gain, and the 19-injection method was chosen. All experiments were performed at a set temperature of 25 °C.

Imaging: Images were acquired with Leica Thunder microscope, using a 10x, NA 0.3 objective, or a 5x, NA 0.12 objective.

Synthesis of 8-arm PEG-NB: The synthesis of 8-arm PEG-norbornene (PEG-NB) was done as published previously.[14] Briefly, 8-arm PEG-NH_2HCl (M_n = 10 000 g mol^{-1}; 8 g, 0.8 mmol PEG, 6.4 mmol NH_2) was dissolved in anhydrous dimethylformamide (DMF; 5 mL). First, *N*,*N*-Diisopropylethylamine (DIPEA; 4.46 mL, 25.6 mmol, 4 eq.) and 1-[bis(dimethylamino)methylene]−1H-1,2,3-triazolo[4,5-b]pyridinium-3-oxide hexafluorophosphate] (HATU; 4.86 g, 12.8 mmol, 2 eq.) were added to the PEG solution. Next, 5-norbornene-2-carboxylic acid; (3.12 mL, 25.6 mmol, 4 eq.; Sigma) was added to the mixture and stirred overnight at room temperature (RT). The reaction mixture was precipitated twice in diethyl ether at 4 °C and the precipitate was dialyzed in a regenerated cellulose dialysis membrane against dH_2O for 3 days. Finally, the polymer solution was frozen and lyophilized.

Fabrication of Bulk Hydrogels: Bulk hydrogels were fabricated using 5–10 wt% 8-arm PEG-NB, 0.287–0.574 wt% dithiothreitol (DTT), and 0.5 wt% lithium-phenyl-2,4,6-trimethylbenzoylphosphinate (LAP) as the photoinitiator. Aliquots of 45 µL pregel solution were pipetted into a 500 µL Eppendorf tube and gelation was achieved via exposure to UV light for 90 s (λ = 365 nm, I = 15 mW cm^{-2}; M365L3-C1, ThorLabs). Bulk hydrogels were then placed into a 50 mL falcon tube filled with PBS for at least 3 days to remove the unreacted precursors and excess LAP by dialysis. PBS was replenished each day during this process. Bulk hydrogels were either used directly after dialysis or stored at 4 °C. In the latter case, PBS was added to the 500 µL Eppendorf tube to prevent hydrogel dehydration.

Rheological Characterization of PEG-NB Networks: Rheometric characterization was performed using a shear rheometer (MCR 502; Anton-Paar; Zofingen, Switzerland) equipped with a Peltier stage to control temperature (T = 25 °C). All data were collected using a sandblasted upper geometry with an 8 mm diameter (PP08/S sandblasted) by Anton Paar. A moist KIMTECH wipe was placed in the measurement chamber to prevent the samples from drying out. Motor adjustments were performed prior to each experiment. Bulk hydrogels were prepared by cross-linking the pregel solution in between the two plates upon UV light exposure for 60 s (λ = 365 nm, I = 15 mW cm^{-2}; M365L3-C1, Thorlabs). Gelation time and storage (G') and loss (G'') moduli were probed via oscillatory tests at γ = 0.1% strain amplitude and an angular frequency of ω = 1 rad s^{-1} that lie in the linear viscoelastic region. Frequency sweep experiments were performed at γ = 0.1% (within the linear viscoelastic regime as determined from strain sweep experiments) for ω = 100–0.01 rad s^{-1}.

Microfluidic Device Fabrication: The microfluidic devices for microgel fabrication and confinement were designed in AutoCAD (Autodesk) and output as high-resolution film shadow masks (Microlitho) for negative photolithography. Master molds were fabricated by spin-coating (WS-650-23B, Laurell) an SU-8 photoresist (GM1070) onto a plasma cleaned silicon wafer (Si-Wafer, Siegert Wafer). The coated layer was soft baked at 65 and 95 °C and patterned by UV exposure through the shadow masks, followed by postbaking (at 65 and 95 °C) and developed using 1-methoxy-2-propyl acetate to remove the unpolymerized photoresist. The wafer was then post-baked at 200 °C for 10 min. Patterned wafers were treated with chlorotrimethylsilane vapor before polydimethylsiloxane (PDMS) molding. Microfluidic devices were fabricated using standard soft-lithographic techniques. A mixture of PDMS monomer and curing agent (Elastosil) at a 9:1 ratio was poured over a silicon wafer mold and peeled off after polymerization at 70 °C for 30 min. Inlets and outlets were punched using a hole puncher (20G Catheter Punch; Schmidt Press), and the PDMS substrate was bonded to a glass slide (Menzel-Glaser, Germany) after oxygen plasma treatment (EMITECH K1000X, Quorum Technologies) of both surfaces for 60 s. Bonded devices were left on a 120 °C hot plate for 2 h to allow complete bonding.

Fabrication of Microgels via Microfluidic Templating: Microgels were fabricated via microfluidic templating of water-in-oil emulsions as previously described.[14] A Cetoni neMESYS (Cetoni GmbH) syringe pump with Cetoni base 120 power adapters were used as displacement syringe pumps for the aqueous and oil phase. A Nikon Eclipse Ts2 (Nikon instruments) inverted microscope paired with uEye Cockpit by iDS7 was used for high-speed imaging of the microfluidic flow. Briefly, hydrogel precursor and oil solutions as described above were loaded into gastight syringes and connected to the inlets of the microfluidic device via Tygon tubing (Cole Palmer GmbH). To form the droplets, the pregel solution was injected into the microfluidic device and pinched off by hydrodynamic focusing between impinging immiscible oil (Droplet generation oil for probes) streams at varying relative volumetric flow rates. The generated droplets were collected in a collection vial with light mineral oil to cap the emulsion and prevent evaporation of the droplet-generation oil. After collection, the droplets were cross-linked via exposure to UV light for 60 s (λ = 365 nm, I = 15 mW cm^{-2}; M365L3-C1, ThorLabs) with LAP as a photoinitiator. Cross-linked microgels were centrifuged at 12 700 rcf for 5 min to separate the three phases. Mineral oil and droplet generation oil were discarded and the microgels were suspended in fivefold excess PBS. Then, the suspension was centrifuged at 12 700 rcf for 5 min and the supernatant removed. This washing cycle was repeated four times.

Fabrication of Microgels via Rotisserie Emulsification: Pregel solutions with DTT (MW = 154 g mol^{-1}) or PEG di-thiol (PEG-dSH) (M_n = 2000 g mol^{-1}) were prepared for the aptamer-functionalized and heparin-functionalized microgels, respectively. In an Eppendorf tube, pregel solutions and fivefold excess droplet generation oil (BioRad) were added. The Eppendorf tube oil was placed on a Thermo Scientific tube revolver (Thermo Scientific). The solution was rotated at 30 rcf for 90 s before being exposed to UV light for 90 s (λ = 365 nm, I = 15 mW cm^{-2}). Cross-linked microgels were centrifuged at 16 000 rcf for 5 min, and then the supernatant was aspirated. The gels were washed twice with 0.0125 wt% Tween20 in PBS at a fivefold excess, and twice with

© 2024 The Author(s). Advanced Healthcare Materials published by Wiley-VCH GmbH

21922659, 2024, 25, Downloaded from https://onlinelibrary.wiley.com/doi/10.1002/adhm.202400800 by Eth Zurich, Wiley Online Library on [15/10/2024]. See the Terms and Conditions (https://onlinelibrary.wiley.com/terms-and-conditions) on Wiley Online Library for rules of use; OA articles are governed by the applicable Creative Commons License

PBS (fivefold excess) bycentrifugation between each wash as described above.

Microgel Size Characterization: Microgels were placed on a microscope slide at a low concentration and imaged in brightfield (20x magnification). The images were then manually fitted with ellipses using ImageJ, and the major axis of the fitted ellipse were measured.

Calibration Curves for Model Biomolecules: A seven-point standard curve using twofold serial dilutions was prepared for each model biomolecule. 2 µL aliquots were measured on a NanoDrop One spectrophotometer. Since the calibration curves for all biomolecules yielded a linear dependence between the measured data and the concentration, linear regression was used to determine concentration.

Biomolecule Sequestration Assays: Sequestration experiments were performed on bulk hydrogels (45 µL) and granular hydrogels (45 mg). Rhodamine B, lysozyme, and fluorescein isothiocyanate labeled bovine serum albumin (FITC-BSA) were used as model biomolecules. The concentrations of biomolecules were measured on a Nanodrop One device. Briefly, experiments involved gel samples to an equal volume of either PBS (as a negative control), or the biomolecule solution, was added. The samples were protected from light incubated under mechanical agitation at room temperature. Aliquots were collected at timepoints of 0, 0.5, 3, 8, 24, 48, and 96 h. Prior to the collection of each timepoint, gels were briefly centrifuged, then pipette-mixed to ensure a homogeneous distribution of the biomolecules in the supernatant, and finally, samples taken. Absorbance from the samples was measured directly on the Nanodrop One.

Aptamer Folding and Disulfide Reduction: Reconstituted IL-6-aptamer solutions (100 µM) were diluted in folding buffer (Cambio UK) at 10x working concentration. The solution was then heated to 95 °C for 5 min to ensure proper folding and allowed to cool to room temperature. Folded aptamers were diluted fivefold to working concentration in equal volume of 10 mM TCEP and incubated for 10 min at room temperature to reduce disulfide bonds and expose thiol groups for hydrogel attachment. Final working solutions at 5 µ were prepared by diluting reduced aptamers to a solution containing and 5 mM $MgCl_2$ in PBS.

Aptamer Attachment to Hydrogels: Equal volume of aptamer working solution was added to the microgels to achieve a final concentration of 2.5 µM in the gels. The mixture was placed on a shaker plate and allowed to incubate overnight. 10 mM TCEP and 0.2 wt% LAP was then added to the mixture and exposed to UV light for 90 s (λ = 365 nm, I = 15 mW cm^{-2}). Functionalized microgels were washed using fivefold excess $MgCl_2$ (1 mM in PBS), with centrifugation at 16 000 rcf for 5 min, for a total of four washes.

Aptamer Staining: IL-6 aptamer-loaded microgels were stained using SYBR-gold nucleic acid stain (Thermo Fisher), diluted 8000-fold in tris(hydroxymethyl)aminomethane ethylenediaminetetraacetic acid (Tris-EDTA) buffer (10 mM Tris-Cl, 1 mM EDTA). The gels were protected from light and incubated in 1 mL staining solution for 20 min under mechanical agitation. Gels were washed four times with fivefold excess PBS and centrifuged at 16 000 rcf for 5 min between washes to remove any excess staining solution prior to imaging.

IL-6 Sequestration and Release Assays: Experiments consisted of bulk and granular DTT-containing, and granular PEG-dSH-containing hydrogels to which equal volume of supernatant (200 ng mL^{-1} IL-6 in 0.1% BSA in PBS) was added in a 500 µL Eppendorf tube. Samples were incubated under mechanical agitation at room temperature. Timepoints were collected at 0, 0.5, 3, 8, 24, and 48 h. At each time point, the samples were briefly centrifuged and diluted 125-fold in sample dilution buffer (0.1% BSA in PBS, 0.2 µm filtered). Samples were stored at −80 °C until quantification. Following a sequestration assay conducted in a 48-well plate, with all other conditions identical to those listed in the previous section a release assay was conducted to determine the efficiency of sequestration, as well as retention of IL-6. IL-6-containing supernatant was aspirated and stored for quantification, and replaced with release media (PBS, 1% BSA). The plate was incubated at room temperature under mechanical agitation, and time points were collected at similar time points to above: 0.5, 3, 8, 24, and 48 h. Plates were centrifuged at 3214 rcf for 5 min before each collection.

VEGF-A Loading and Release Assays: PEG-dSH-containing and DTT-containing granular hydrogels were prepared using the rotisserie emulsification method as mentioned above. Equal volume of 5 µm heparin-thiol (heparin-SH, MW = 27 kDa) solution was added to the gels. The gels were then protected from direct exposure to light and incubated overnight under mechanical agitation at room temperature. The next day, 10 mM TCEP was added to reduce any dimerized heparin, and the gels were incubated for 30 min. 0.2 wt% LAP was then added, and the heparin-SH was attached to the gels via exposure to UV light for 5 min (λ = 365 nm, I = 15 mW cm^{-2}). The gels were then centrifuged at 16 000 rcf for 5 min and the supernatant was removed. Fivefold excess volume of PBS was added to wash the gels for a total of four washes, centrifuging as mentioned above between each wash. VEGF-A at 500 ng mL^{-1} was prepared in PBS and added to the gels, with Fourfold excess volume ratio. The gels were allowed to sequester the VEGF-A overnight at room temperature under agitation. The next day, the supernatant was aspirated, and the gels were transferred to a 48 well-plate via a positive displacement pipette. Fourfold excess volume of PBS with 1% BSA was added to facilitate biomolecule release. At predetermined time points, namely 24, 48, 120, and 288 h, the release media was collected and stored at −80 °C for further quantification. The collected volume was replaced with fresh PBS.

Simultaneous Release and Sequestration Assays: Granular hydrogels were prepared as mentioned above. DTT-containing microgels were functionalized with IL-6 aptamer for IL-6 sequestration (termed A microgels below) and PEG-dSH-containing microgels were heparin-SH functionalized and loaded with 500 ng mL^{-1} VEGF-A (termed H microgels below). Once prepared, the two microgel populations were mixed together in an Eppendorf tube using a positive displacement pipette at five different ratios: 100% A:0% H, 80% A:20% H, 50% A:50% H, 20% A:80% H, 0% A:100%. The microgels were then transferred to a 48 well-plate, and fourfold excess volume of IL-6 containing media (500 ng mL^{-1} IL-6 in PBS +1% BSA, +1% penicillin/streptomycin) was added to initiate IL-6 sequestration and VEGF-A release. The plate was incubated at 37 °C in a humidified atmosphere at 5% CO_2 under agitation at 90 rpm. Timepoints were collected at 48 and 120 h, and samples were either stored at −80 °C until quantification or used immediately for cell-based assays.

IL-6 Enzyme-Linked Immunosorbent Assay (ELISA): The quantification of IL-6 was determined using a solid phase sandwich ELISA, following the manufacturer's instructions. Briefly, 100 µL of capture antibody (diluted to 2 µg mL^{-1} in PBS) was added to each well in a 96-well plate and incubated overnight at 4 °C. Following incubation, the plate was washed three times with 300 µL of wash buffer (0.05% Tween20 in TBS, pH adjusted to 7.2–7.4). 300 µL of blocking buffer (2% BSA in wash buffer, 0.2 µm filtered) was then added to each well and the plate was incubated for 1 h at room temperature under mechanical agitation. After a washing step, 100 µL of samples diluted in dilution buffer (0.1% BSA in wash buffer, pH 7.2–7.4, 0.2 µm filtered) were added to each well and the plate was incubated for 2 h at room temperature under mechanical agitation. After another washing step, 100 µL of the horseradish peroxidase (HRP) conjugated IL-6 monoclonal detection antibody (diluted to 0.25 µg mL^{-1} in dilution buffer) was added to each well and incubated for 1 h at room temperature under mechanical agitation. After a final washing step, 200 µL of substrate solution (0.1 mg mL^{-1} TMB and 0.0024% H_2O_2 in 0.05 M Na_2HPO_4 and 0.025 M citric acid buffer, pH adjusted to 5.5) was added to each well and the sealed plate was covered in foil and incubated for 20 min at room temperature under mechanical agitation and protected from direct exposure to light. Finally, 50 µL of stop solution (2 M H_2SO_4) was added to quench the reaction. A HIDEX Sense microplate reader (HIDEX) was used to measure absorbance at λ = 450 nm.

VEGF-A ELISA: VEGF-A was quantified via a solid phase sandwich ELISA, following the manufacturer's instructions. Each well in a 96-well plate was coated with 100 µL capture antibody diluted to 0.15 µg mL^{-1} in PBS and left to incubate overnight at 4 °C. The next day, the plate was washed three times with 300 µL of wash buffer (0.05% Tween20 in TBS, pH adjusted to 7.2–7.4). The plate was then blocked using 300 µL of blocking buffer (2% BSA in wash buffer, 0.2 µm filtered) and incubated for 1 h under mechanical agitation. Following three more washes, 100 µL of samples were added to each well (prediluted in dilution buffer; 0.1% BSA in

© 2024 The Author(s). Advanced Healthcare Materials published by Wiley-VCH GmbH

21922659, 2024, 25, Downloaded from https://onlinelibrary.wiley.com/doi/10.1002/adhm.202400800 by Eth Zurich, Wiley Online Library on [15/10/2024]. See the Terms and Conditions (https://onlinelibrary.wiley.com/terms-and-conditions) on Wiley Online Library for rules of use; OA articles are governed by the applicable Creative Commons License

Table 1. List of primers used for gene expression.

Gene target	Forward primer	Reverse primer
IL-6	5′- GATTCAATGAGGAGACTTGCC -3′	5′- TGTTCTGGAGGTACTCTAGGT -3′
SOCS3	5′- CCTGCGCCTCAAGACCTTC -3′	5′- GTCACTGCGCTCCAGTAGAA -3′
IL-8	5′- GAGAGTGATTGAGAGTGGACCAC -3′	5′- CACAACCCTCTGCACCCAGTTT -3′
MMP1	5′- AAAATTACACGCCAGATTTGCC -3′	5′- GGTGTGACATTACTCCAGAGTTG -3′
RPL27	5′- CGGAAGTGTCCTTCTTTCCTTT -3′	5′- GCCATCATCAATGTTCTTCACG -3′

wash buffer, pH 7.2–7.4, 0.2 µm filtered) was added to each well and incubated for 2 h under mechanical agitation. Another washing step followed, after which 100 µL of detection antibody was diluted to 0.15 µg mL^{-1} in detection antibody dilution buffer (0.5% BSA in wash buffer, pH 7.2–7.4, 0.2 µm filtered) and incubated for 1 h at room temperature, under mechanical agitation. After a final washing step, 200 µL of substrate solution (0.1 mg mL^{-1} TMB and 0.0024% H_2O_2 in 0.05 M Na_2HPO_4 and 0.025 M citric acid buffer, pH adjusted to 5.5) was added to each well and incubated for 20 min at room temperature under mechanical agitation and protected from direct exposure to light. Finally, 50 µL of stop solution (2 M H_2SO_4) was added to quench the reaction. A HIDEX Sense microplate reader (HIDEX) was used to carry out the read-out, at $\lambda = 450$ nm absorbance.

HaCaT Cell Culture: Human immortalized epidermal keratinocytes (HaCaT) were expanded and maintained in basal media Dulbecco's Modified Eagle Medium (DMEM) (4.5 g L^{-1} Glucose) (Gibco) supplemented with 10% fetal bovine serum (FBS) (Gibco), and 1% PenStrep. Cells were passaged using 0.05% Trypsin-EDTA (Gibco) at ≈ 90% confluence. All cultures were grown at 37 °C in a humidified atmosphere at 5% CO_2 (Binder) with medium change every 2 days. Treatment with cytokines were performed by the addition of IL-6 (20 ng mL^{-1}) or TNF-α (10 ng mL^{-1}) diluted in cell media.

Transwell Assays: Experiments were performed on HaCaT cells cultured in the basolateral compartment of a 24 well plate at 50k cells per well under control or inflammatory conditions. Transwells were prepared using plate inserts, to which 100 µL of microgels were added. For sequestration experiments, 120 µL of media was aspirated from the basolateral compartment, and frozen, before being replenished using control or treated media. Between timepoint collection, the plate was kept at 37 °C in a humidified atmosphere at 5% CO_2 under agitation via an orbital shaker. Release experiments were carried out via transfer of transwell inserts to a 24 well plate with 600 µL PBS per well. All of the release media was collected at specified timepoints, and frozen, before being replenished. Between timepoint collection, the plate was subject to the same conditions as mentioned for sequestration. Results were analyzed via ELISA.

Gene Expression: Cell cultures were collected in TriZOL (Thermofisher). RNA was isolated using phase separation. RNA was purified and quantified using a Nanodrop One C. Reverse Transcription was performed using High-Capacity Reverse Transcriptase (Thermofisher) to obtain cDNA. Gene expression was measured by real-time quantitative PCR (RT-qPCR) using SYBR-Green (Thermofisher) on a QuantStudio 3. Primers were obtained from Microsynth (**Table 1**). Gene expression was quantified relative to RPL27 using the $\Delta\Delta C_T$ method and normalized to the control condition.

HEK-Blue Cell Assays: Human embryonic kidney (HEK) IL-6 sensor cells were purchased from Invivogen (Cat # hkb-hil6). These cells are transfected with a reporter gene expressing secreted alkaline phosphatase (SEAP) under the control of a STAT3 sensitive promoter. With IL-6 signaling, the JAK-STAT pathway is activated leading to SEAP expression. SEAP can be detected by absorbance assays. HEK-Blue cells were cultured in Dulbecco's Modified Eagle Medium (DMEM) (4.5 g L^{-1} Glucose) (Gibco) supplemented with 10% heat-inactivated fetal bovine serum (FBS) (Gibco), and 1% PenStrep. During the growth phase, normocin and selection antibiotics were added to the media (removed for the testing). For testing IL-6 activity, HEK-Blue cells were seeded at 50 000 cells per well in a 96-well plate. Supernatant from the sequestration and release assay was diluted in media to be in the detectable range and added to the wells (1:10 v/v). Cells were incubated with this supernatant for 24 h. 20 µL supernatant was collected and added to 180 µL of QuantiBlue detection reagent (Invivogen, rep-qbs). The mixture was incubated for 1–3 h at 37 °C after which the absorbance was measured at $\lambda = 637$ nm. A representative standard curve is shown in Figure S9 (Supporting Information).

HUVEC Growth Assays: Green fluorescent protein labeled human umbilical vascular endothelial cells (GFP-HUVECs) were cultured in Modified Eagle Medium α (Sigma), supplemented with 10% FBS, Glutamax (Gibco) and 50 ng mL^{-1} fibroblast growth factor 2 (FGF-2) on gelatin-coated flasks. Cells were seeded at 10 000 cells per well on a noncoated 96-well plate in media (without FGF-2) with supernatants from the sequestration and release experiments. The supernatant was supplemented with 10% FBS before applying it to the cells. Cell growth and spreading was measured at 48 h by fluorescent imaging of GFP signal in the whole well. Total cell spread area was measured with ImageJ.

Statistical Tests: Statistical analysis was performed using Origin Pro 2023 (OriginLab Corporation). Unless otherwise stated, statistical significance was determined by T tests. For comparisons between groups, one way ANOVA with a Tukey post-hoc test was performed. Performed tests and significance levels are indicated in the corresponding figure captions.

Supporting Information

Supporting Information is available from the Wiley Online Library or from the author.

Acknowledgements

The authors would like to thank the Ehrbar group (University of Zurich) for their kind donation of HUVEC-GFP cells. ITC was performed on the equipment of Prof. Nyström's lab (ETH Zurich), with the support of Dr. Cristina Lupo. This work was supported by ETH Zurich (startup funds to M.W.T.), the Helmut Horten Stiftung (M.W.T.), and ETH Open project SKINTEGRITY.CH (M.W.T.).

Open access funding provided by Eidgenossische Technische Hochschule Zurich.

Conflict of Interest

D.B.E., A.S., B.M.D., N.S., C.L., and M.W.T. are co-inventors of a patent application related to the research in this manuscript.

Author Contributions

The project was conceived of and designed by D.B.E., B.M.D., A.J.dM, C.L., and M.W.T. The experiments were carried out by D.B.E, B.M.D., C.L., A.S., N.S., and N.N. Transport model was developed by D.B.E, B.M.D., and P.G.R. The rotisserie emulsion method for microgel fabrication was developed by J.S.O. The manuscript was written by D.B.E., A.S., A.J.dM, C.L., and M.W.T. All authors have approved the final version of the manuscript.

© 2024 The Author(s). Advanced Healthcare Materials published by Wiley-VCH GmbH

21922659, 2024, 25, Downloaded from https://onlinelibrary.wiley.com/doi/10.1002/adhm.202400800 by Eth Zurich, Wiley Online Library on [15/10/2024]. See the Terms and Conditions (https://onlinelibrary.wiley.com/terms-and-conditions) on Wiley Online Library for rules of use; OA articles are governed by the applicable Creative Commons License

Data Availability Statement

The data that support the findings of this study are available from the corresponding author upon reasonable request.

Keywords

biomaterials, biomolecule release, biomolecule sequestration, cytokines, granular hydrogels, immunomodulation, wound healing

Received: February 29, 2024
Revised: May 7, 2024
Published online: June 10, 2024

[1] S. A. Eming, P. Martin, M. Tomic-Canic, *Sci. Transl. Med.* **2014**, *6*, 265sr6.
[2] J. L. Zakrzewski, M. R. M. van den Brink, J. A. Hubbell, *Nat. Biotechnol.* **2014**, *32*, 786.
[3] J. Larouche, S. Sheoran, K. Maruyama, M. M. Martino, *Adv. Wound Care* **2018**, *7*, 209.
[4] G. Hübner, M. Brauchle, H. Smola, M. Madlener, R. Fässler, S. Werner, *Cytokine* **1996**, *8*, 548.
[5] R. Augustine, N. Kalarikkal, S. Thomas, *Prog. Biomater.* **2014**, *3*, 103.
[6] V. Falanga, S. Iwamoto, M. Chartier, T. Yufit, J. Butmarc, N. Kouttab, D. Shrayer, P. Carson, *Tissue Eng.* **2007**, *13*, 1299.
[7] M. Kharaziha, A. Baidya, N. Annabi, *Adv. Mater.* **2021**, *33*, 2100176.
[8] S. Dixit, D. R. Baganizi, R. Sahu, E. Dosunmu, A. Chaudhari, K. Vig, S. R. Pillai, S. R. Singh, V. A. Dennis, *J. Biol. Eng.* **2017**, *11*, 49.
[9] M. Rodrigues, N. Kosaric, C. A. Bonham, G. C. Gurtner, *Physiol. Rev.* **2019**, *99*, 665.
[10] M. P. Lutolf, J. A. Hubbell, *Nat. Biotechnol.* **2005**, *23*, 47.
[11] A. K. Gaharwar, I. Singh, A. Khademhosseini, *Nat. Rev. Mater.* **2020**, *5*, 686.
[12] C. Ligorio, A. Mata, *Nat. Rev. Bioeng.* **2023**, *1*, 518.
[13] T. H. Qazi, J. A. Burdick, *Biomater. Biosyst.* **2021**, *1*, 100008.
[14] D. B. Emiroglu, A. Bekcic, D. Dranseikiene, X. Zhang, T. Zambelli, A. J. deMello, M. W. Tibbitt, *Sci. Adv.* **2022**, *8*, eadd8570.
[15] A. Puiggalí-Jou, M. Asadikorayem, K. Maniura-Weber, M. Zenobi-Wong, *Acta Biomater.* **2023**, *166*, 69.
[16] T. H. Qazi, V. G. Muir, J. A. Burdick, *ACS Biomater. Sci. Eng.* **2022**, *8*, 1427.
[17] D. R. Griffin, W. M. Weaver, P. O. Scumpia, D. Di Carlo, T. Segura, *Nat. Mater.* **2015**, *14*, 737.
[18] D. R. Griffin, M. M. Archang, C.-H. Kuan, W. M. Weaver, J. S. Weinstein, A. C. Feng, A. Ruccia, E. Sideris, V. Ragkousis, J. Koh, M. V. Plikus, D. Di Carlo, T. Segura, P. O. Scumpia, *Nat. Mater.* **2021**, *20*, 560.
[19] S. Mohammadi, H. Ravanbakhsh, S. Taheri, G. Bao, L. Mongeau, *Adv. Healthcare Mater.* **2022**, *11*, e2102366.
[20] L. Pruett, C. Jenkins, N. Singh, K. Catallo, D. Griffin, *Adv. Funct. Mater.* **2021**, *31*, 2104337.
[21] P. S. Briquez, J. A. Hubbell, M. M. Martino, *Adv. Wound Care* **2015**, *4*, 479.
[22] M. M. Martino, P. S. Briquez, A. Ranga, M. P. Lutolf, J. A. Hubbell, *Proc. Natl. Acad. Sci. USA* **2013**, *110*, 4563.
[23] J. A. Hubbell, S. N. Thomas, M. A. Swartz, *Nature* **2009**, *462*, 449.
[24] D. Hachim, T. E. Whittaker, H. Kim, M. M. Stevens, *J. Controlled Release* **2019**, *313*, 131.
[25] J. Ishihara, A. Ishihara, K. Fukunaga, K. Sasaki, M. J. V. White, P. S. Briquez, J. A. Hubbell, *Nat. Commun.* **2018**, *9*, 2163.
[26] N. Lohmann, L. Schirmer, P. Atallah, E. Wandel, R. A. Ferrer, C. Werner, J. C. Simon, S. Franz, U. Freudenberg, *Sci. Transl. Med.* **2017**, *9*, eaai9044.
[27] H. Ryoo, G. H. Underhill, *ACS Biomater. Sci. Eng.* **2023**, *9*, 2317.
[28] S. Boesveld, Y. Kittel, Y. Luo, A. Jans, B. Oezcifci, M. Bartneck, C. Preisinger, D. Rommel, T. Haraszti, S. P. Centeno, A. J. Boersma, L. De Laporte, C. Trautwein, A. J. C. Kuehne, P. Strnad, *Adv. Healthcare Mater.* **2023**, *12*, e2300695.
[29] J. Li, D. J. Mooney, *Nat. Rev. Mater.* **2016**, *1*, 16071.
[30] M. E. Young, P. A. Carroad, R. L. Bell, *Biotechnol. Bioeng.* **1980**, *22*, 947.
[31] W. Grellner, T. Georg, J. Wilske, *Forensic. Sci. Int.* **2000**, *113*, 251.
[32] A. Ruscito, M. C. DeRosa, *Front. Chem.* **2016**, *4*, 14.
[33] N. Nakatsuka, A. Faillétaz, D. Eggemann, C. Forró, J. Vörös, D. Momotenko, *Anal. Chem.* **2021**, *93*, 4033.
[34] B. Shkodra, M. Petrelli, K. Yang, A. Tagliaferri, P. Lugli, L. Petti, N. Nakatsuka, *Faraday Discuss.* **2024**, *250*, 43.
[35] E. Adrian, D. Trelová, E. Filová, M. Kumorek, V. Lobaz, R. Poreba, O. Janoušková, O. Pop-Georgievski, I. Lacík, D. Kubies, *Int. J. Mol. Sci.* **2021**, *22*, 11666.
[36] J. Koh, D. R. Griffin, M. M. Archang, A.-C. Feng, T. Horn, M. Margolis, D. Zalazar, T. Segura, P. O. Scumpia, D. Di Carlo, *Small* **2019**, *15*, e1903147.
[37] A. R. Anderson, E. Nicklow, T. Segura, *Acta Biomater.* **2022**, *150*, 111.
[38] E. G. Lee, L. R. Luckett-Chastain, K. N. Calhoun, B. Frempah, A. Bastian, R. M. Gallucci, *J. Immunol. Res.* **2019**, *2019*, 5087847.
[39] M. A. Nosenko, S. G. Ambaryan, M. S. Drutskaya, *Mol. Biol.* **2019**, *53*, 653.
[40] L. Pruett, R. Ellis, M. McDermott, C. Roosa, D. Griffin, *J. Mater. Chem. B* **2021**, *9*, 7132.
[41] A. C. Lima, C. Cunha, A. Carvalho, H. Ferreira, N. M. Neves, *ACS Appl. Mater. Interfaces* **2018**, *10*, 13839.
[42] L. A. Krattiger, D. B. Emiroglu, S. Pravato, L. O. Moser, O. A. Bachmann, S. Y. La Cioppa, G. J. R. Rivera, J. A. Burdick, A. J. deMello, M. W. Tibbitt, M. Ehrbar, *Adv. Funct. Mater.* **2024**, https://doi.org/10.1002/adfm.202310507.

© 2024 The Author(s). Advanced Healthcare Materials published by Wiley-VCH GmbH

21922659, 2024, 25, Downloaded from https://onlinelibrary.wiley.com/doi/10.1002/adhm.202400800 by Eth Zurich, Wiley Online Library on [15/10/2024]. See the Terms and Conditions (https://onlinelibrary.wiley.com/terms-and-conditions) on Wiley Online Library for rules of use; OA articles are governed by the applicable Creative Commons License